Annals of Nuclear Medicine Vol. 20, No. 6, 409–416, 2006

Use of a compact pixellated gamma camera for small animal pinhole SPECT imaging

Tsutomu ZENIYA,* Hiroshi WATABE,* Toshiyuki AOI,* Kyeong Min KIM,** Noboru TERAMOTO,* Takeshi TAKENO,* Yoichiro OHTA,* Takuya HAYASHI,* Hiroyuki MASHINO,*** Toshihiro OTA,*** Seiichi YAMAMOTO**** and Hidehiro IIDA*

*Department of Investigative Radiology, Advanced Medical Engineering Center, National Cardiovascular Center Research Institute
**Nuclear Medicine Laboratory, Radiological and Medical Sciences Research Center, Korea Institute Radiological and Medical Sciences
***Molecular Imaging Laboratory, Inc.
****Department of Electrical Engineering, Kobe City College of Technology

Objectives: Pinhole SPECT which permits *in vivo* high resolution 3D imaging of physiological functions in small animals facilitates objective assessment of pharmaceutical development and regenerative therapy in pre-clinical trials. For handiness and mobility, the miniature size of the SPECT system is useful. We developed a small animal SPECT system based on a compact high-resolution gamma camera fitted to a pinhole collimator and an object-rotating unit. This study was aimed at evaluating the basic performance of the detection system and the feasibility of small animal SPECT imaging. ***Methods:*** The gamma camera consists of a 22 × 22 pixellated scintillator array of 1.8 mm × 1.8 mm × 5 mm NaI(Tl) crystals with 0.2-mm gap between the crystals coupled to a 2″ flat panel position-sensitive photomultiplier tube (Hamamatsu H8500) with 64 channels. The active imaging region of the camera was 43.8 mm × 43.8 mm. Data acquisition is controlled by a personal computer (Microsoft Windows) through the camera controller. Projection data over 360° for SPECT images are obtained by synchronizing with the rotating unit. The knife-edge pinhole collimators made of tungsten are attached on the camera and have 0.5-mm and 1.0-mm apertures. The basic performance of the detection system was evaluated with ^{99m}Tc and ^{201}Tl solutions. Energy resolution, system spatial resolution and linearity of count rate were measured. Rat myocardial perfusion SPECT scans were sequentially performed following intravenous injection of ^{201}TlCl. Projection data were reconstructed using a previously validated pinhole 3D-OSEM method. ***Results:*** The energy resolution at 140 keV was 14.8% using a point source. The system spatial resolutions were 2.8-mm FWHM and 2.5-mm FWHM for ^{99m}Tc and ^{201}Tl line sources, respectively, at 30-mm source distance (magnification factor of 1.3) using a 1.0-mm pinhole. The linearity between the activity and count rate was good up to 10 kcps. In a rat study, the left ventricular walls were clearly visible in all scans. ***Conclusions:*** We developed a compact SPECT system using compact gamma camera for small animals and evaluated basic physical performances. The present system may be of use for quantitation of biological functions such as myocardial blood flow in small animals.

Key words: SPECT, pinhole collimator, compact pixellated gamma camera, small animal

Received February 3, 2006, revision accepted May 10, 2006.
For reprint contact: Tsutomu Zeniya, Ph.D., Department of Investigative Radiology, Advanced Medical Engineering Center, National Cardiovascular Center Research Institute, 5–7–1 Fujishiro-dai, Suita, Osaka 565–8565, JAPAN.
E-mail: zeniya@ri.ncvc.go.jp

INTRODUCTION

SMALL ANIMAL PET (Positron Emission Tomography) or SPECT (Single Photon Emission Computed Tomography) which permits *in vivo* high resolution three-dimensional (3D) imaging of physiological functions in small laboratory animals, facilitates objective assessment of pharmaceutical development and regenerative therapy in pre-clinical trials.[1–6] Small animal PET has been widely used due to high spatial resolution approaching 1 mm.[7–9] SPECT can also offer high-resolution images by attaching a pinhole collimator with a large magnification factor, when the object is placed close to the pinhole.[10–13] Spatial resolution is improved particularly when a small diameter pinhole is employed.[14–17]

However, a conventional pinhole SPECT has two major limitations. One is its poor sensitivity as compared with small animal PET. The sensitivity of pinhole SPECT is in the order of 1/100–1/1,000 of that of small animal PET, depending on the pinhole diameter, but can be improved by positioning the pinhole collimator close to the object, or by using multiple-detector systems or multiple-pinhole systems.[14,15,17,19,20] Another limitation is the non-uniformity of spatial resolution in the reconstructed 3D images. In pinhole SPECT, the spatial resolution is axially blurred with increased distance from the midplane. This non-uniformity of spatial resolution can be improved by complete data acquisition as demonstrated in our earlier study.[18]

Besides high spatial resolution, the SPECT system has several advantages over PET as its operation is simple, and it does not require an on-site radiochemistry laboratory or a cyclotron for producing radiopharmaceuticals. Pinhole SPECT systems are often composed of clinically used SPECT cameras with pinhole collimator.[3–6,10–15,18,20] However, the clinically used SPECT cameras are inappropriate for small animal imaging, largely due to a lack of manufacturing precision. Also they are not readily accessible to most animal research laboratories.[22]

To overcome these drawbacks, several dedicated small animal pinhole SPECT systems using compact high-resolution gamma cameras have been already developed.[23–25] They used 5″ position-sensitive photomultiplier tube (PSPMT) which had the camera active image region of around 100 mm × 100 mm. In this study, we have employed more a compact pixellated gamma camera with active image region of 43.8 mm × 43.8 mm square coupled to 2″ PSPMT and have developed a compact pinhole SPECT system dedicated to small animal imaging. This study was aimed at evaluating the basic physical performances and the feasibility of small animal imaging in this compact SPECT system.

MATERIALS AND METHODS

Detection system description

The gamma camera consists of a 22 × 22 pixellated scintillator array of 1.8 mm × 1.8 mm × 5 mm NaI(Tl) crystals with 0.2-mm white epoxy gap of diffuse, opaque reflective material between the crystals (Fig. 1 (a)) optically coupled to a 2″ flat PSPMT (Hamamatsu H8500) with 64 channel anodes (Fig. 1 (b)). The scintillator array has a 0.5-mm aluminum window and 2-mm glass window on gamma-ray input and light output sides, respectively. The active imaging region of the camera was 43.8 mm × 43.8 mm square.

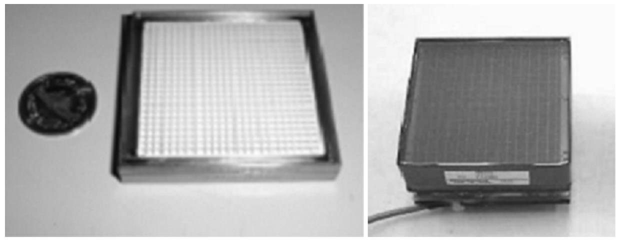

a b

Fig. 1 (a) Photograph of pixellated NaI scintillator array. (b) Photograph of 2-inch flat panel position-sensitive photomultiplier tube.

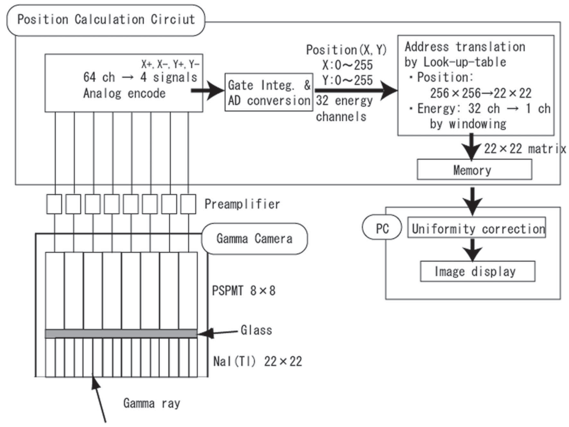

Fig. 2 Schematic diagram of position calculation circuit.

Figure 2 shows a schematic diagram of a position calculation circuit. Analog outputs from 64 PSPMTs through preamplifiers are weighted in proportion to coordinates and are summed in X+, X−, Y+ and Y− directions. After applying gated integration and analog-to-digital conversion for these encoded four analog outputs, the position is obtained by calculating the center of the gravity from the four signals, and is assigned to either pixel in 256 × 256 matrix as a raw image. Also an energy spectrum with 32 channels is collected for each pixel. And then, by address translation using look-up-table (LUT), the raw image of 256 × 256 × 32 matrix is converted to 22 × 22 × 1 image matrix according to the number of scintillators and energy window described below. The counts within the region divided by 22 × 22-matrix grid are summed. The positions of horizontal and vertical lines of the grid are alterable by the interactive tool (Fig. 3) on a personal computer (Windows 2000 (Microsoft)) (PC). Thus, all events are assigned to a 1.8 mm × 1.8 mm crystal in the image matrix. On the other hand, the energy window is set as above and below channel widths from a photopeak channel searched in each pixel. We assume the use of two radioisotopes of ^{99m}Tc and ^{201}Tl. The main photopeaks are 140 keV and 70 keV for ^{99m}Tc and ^{201}Tl, respectively. Here, the camera gain for ^{201}Tl was set about twice as much as that for ^{99m}Tc. The energy width with each channel corresponds to approximately 10 keV and 5 keV for ^{99m}Tc and ^{201}Tl, respectively. The energy window was actually set at five channels, namely, approximately 36% for both ^{99m}Tc and ^{201}Tl and centered on the photopeak channel searched. Finally, the converted 22 × 22-pixel image is stored on memory and then is transferred to the PC. The PC can perform several tasks such as correcting uniformity, displaying and analyzing images. Figure 3 shows flood raw image by irradiating with a ^{99m}Tc point source. Separation between pixels was well performed except for pixels in columns and rows at the edge. The effective image field-of-view (FOV) that does not enclose the edge pixels was 20 × 20 pixels (or 39.8 mm × 39.8 mm). The resulting image is used as correction matrix to correct for non-uniformity in sensitivity over camera's FOV.

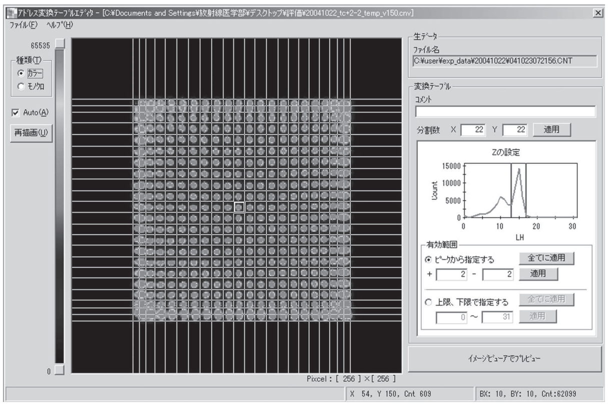

Fig. 3 Interactive tool on PC for making address translation table. The flood raw image was obtained by irradiating with a ^{99m}Tc point source. The separation between pixels was well performed.

Collimator design

As shown in Figures 4 (a) and (b), the pinhole collimator made of tungsten is attached on the gamma camera and has a 0.5-mm or 1.0-mm aperture, 60° opening angle and 39.57-mm focal length. The collimator has a flat face of the single knife-edge pinhole, in order to achieve higher sensitivity and spatial resolution (larger magnification factor) by positioning the pinhole closer to the object. The camera is shielded by tungsten to avoid the penetration of the photon from the surrounding area.

Projection image acquired with the pinhole collimator has non-uniform sensitivity distribution due to the pinhole geometry.[24,25] This non-uniformity can be corrected by using a correction matrix derived from a flood source contained in a thin plate. Figure 4 (c) shows a projection image obtained from the flood source. The correction matrix from this projection image, which has high counts around the center and low counts at the periphery, was actually used to correct the non-uniformity of pinhole sensitivity.

SPECT FOV, namely, the diameter of reconstruction sphere is expressed as:

$$FOV = 2b \sin\left(\frac{\alpha}{2}\right), \qquad (1)$$

where b is the distance from the pinhole to the rotation center of the object (radius of rotation: ROR), α is the opening angle of the pinhole collimator. However, when the diameter of the effective image region of camera c_e is shorter than the diameter of the collimator base c, SPECT FOV_e (effective FOV) is expressed as:

$$FOV_e = \frac{c_e}{c} FOV. \qquad (2)$$

In this collimator c_e of 39.8 mm is shorter than c of 45.69 mm. Therefore, when b is 30 mm, FOV_e becomes 26.1 mm.

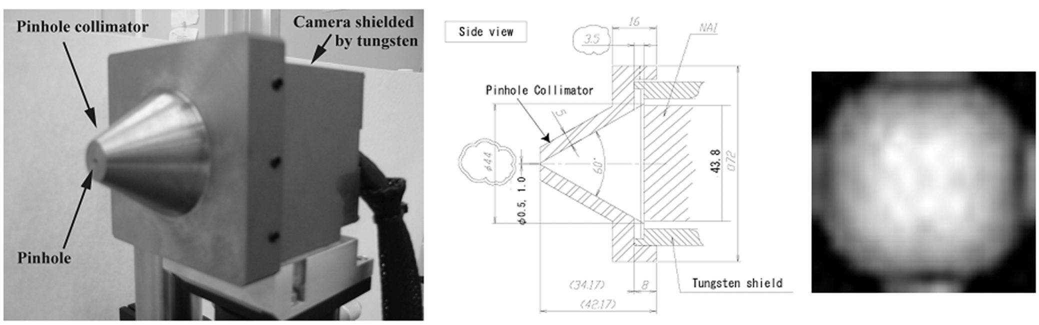

a b c

Fig. 4 (a) Photograph of the pinhole collimator attached to the compact gamma camera. (b) Drawing of side view of the pinhole collimator. (c) Sensitivity map of pinhole collimator. This map was obtained from a flood source filled in a thin plate parallel to the detector and was used to correct non-uniformity of pinhole sensitivity.

SPECT imaging system

Figure 5 shows the pinhole SPECT acquisition system using a compact gamma camera. Data acquisition is controlled by the PC through the camera controller. The rotation of the object stage is synchronized to step and shoot acquisition of the SPECT camera.

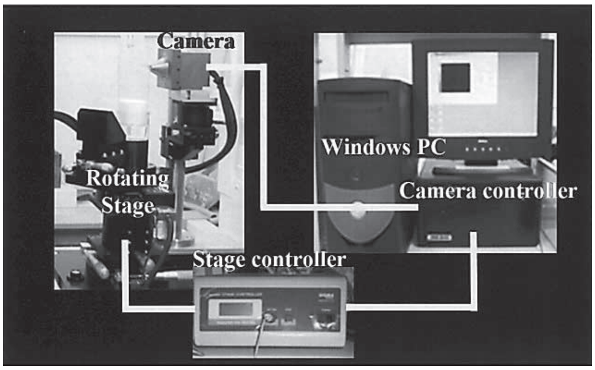

Fig. 5 Pinhole SPECT acquisition system using compact gamma camera. This system consists of compact gamma camera with pinhole collimator, camera controller, PC, object rotating stage and stage controller.

Basic system performances

The performances of the detection system such as the energy resolution, system spatial resolution, sensitivity and linearity of the count rate were examined with ^{99m}Tc (140 keV) and ^{201}Tl (70 keV) sources.

(1) Energy resolution: Energy resolution was measured by uniform irradiation with a 2.18 MBq ^{99m}Tc point source placed at 2 m distant from the camera without the collimator for 12 hours and is defined for each crystal's energy spectrum as full width at half maximum (FWHM) of the photopeak divided by its amplitude. The energy resolution was obtained from an energy spectrum for one crystal near the center of the camera.

(2) System spatial resolution: The FWHMs of the line spread functions (LSFs) were measured in planar image using ^{99m}Tc and ^{201}Tl line sources with 1.14-mm inner diameter placed at 30 mm distant from the 1-mm pinhole. The magnification factor was 1.32. The LSFs of line sources were computed by deconvoluting with rectangular function of 1.14-mm width. The spatial resolutions were defined as the FWHM of Gaussian function obtained from this deconvolution.

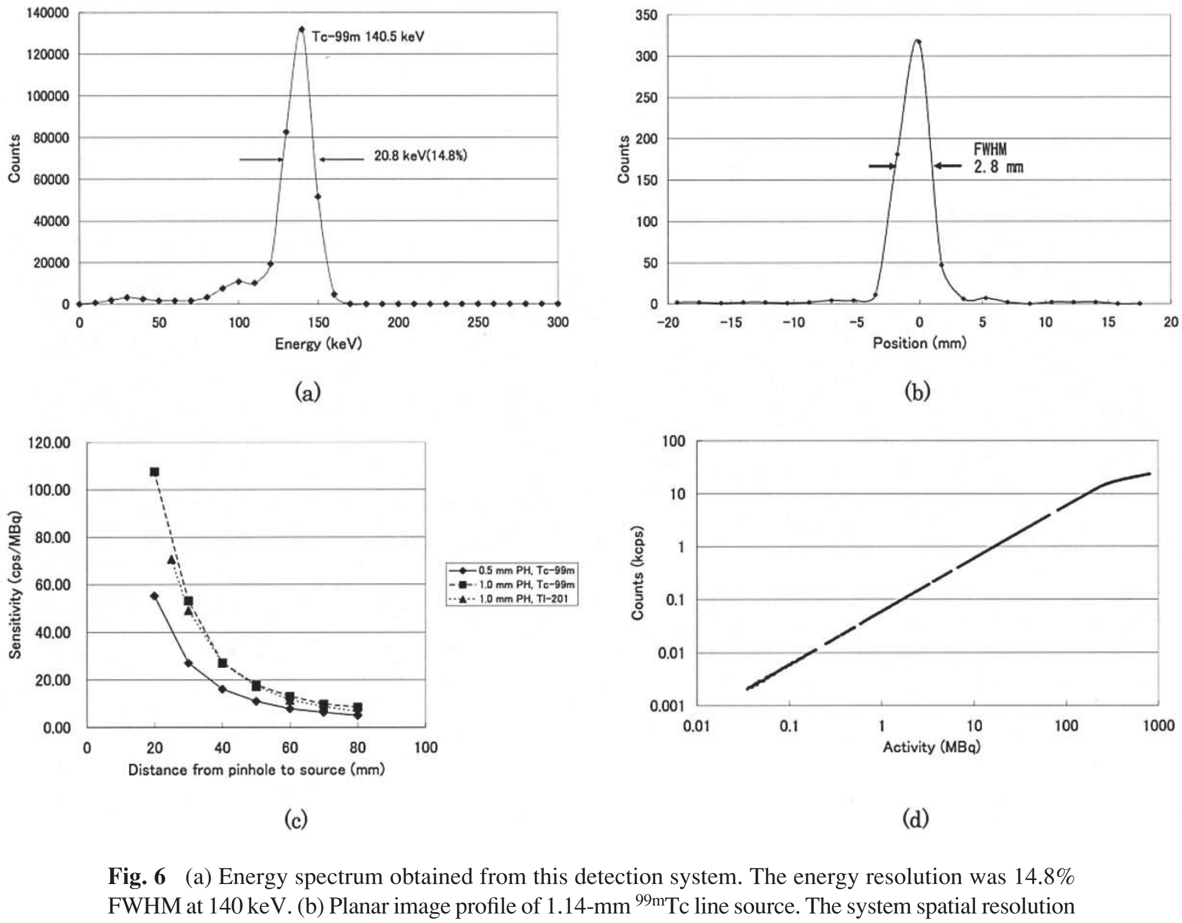

Fig. 6 (a) Energy spectrum obtained from this detection system. The energy resolution was 14.8% FWHM at 140 keV. (b) Planar image profile of 1.14-mm ^{99m}Tc line source. The system spatial resolution obtained from the LSF was 2.8-mm FWHM. (c) On-axis sensitivities for ^{99m}Tc or ^{201}Tl as a function of distance from the pinhole for 0.5-mm or 1.0-mm diameters. (d) Relationship between the source activity and the count rate measured by following decay of ^{99m}Tc source.

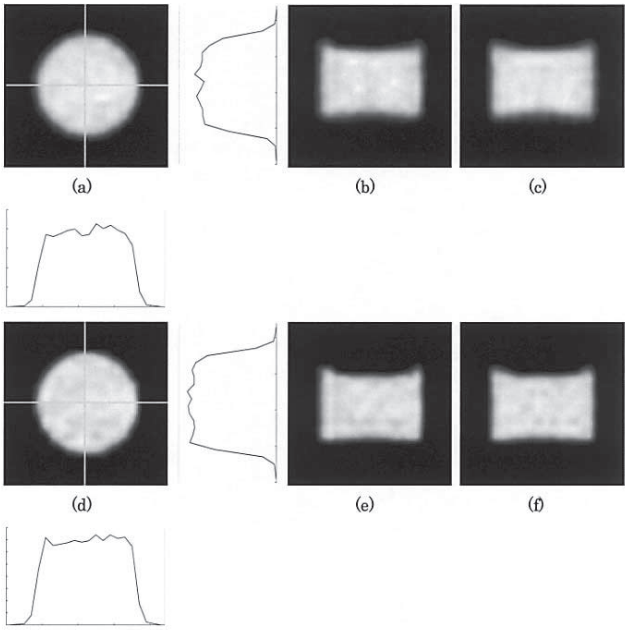

Fig. 7 SPECT images of uniform cylindrical phantom. (a)–(c) are without pinhole sensitivity correction. (d)–(f) are with the correction. (a) and (d) are transverse images. (b) and (e) are coronal images. (c) and (f) are sagittal images. The profiles in the x and y directions were attached to the transverse images of (a) and (d).

(3) Sensitivity: The system sensitivity on the central axis was measured using a small cylindrical phantom of 0.1 ml at eight points in the range from 20 to 80-mm distances with 0.5- or 1.0-mm pinholes and ^{99m}Tc or ^{201}Tl sources.

(4) Linearity of count rate: The counts per 10 min were sequentially measured by following decay of the ^{99m}Tc source. The cylindrical phantom made of glass with 24.3-mm outer diameter and 21.8-mm inner diameter was filled with uniform ^{99m}Tc solution. The center of the phantom was positioned at 30 mm distant from the 1-mm pinhole. Consequently, the relationship between activity and detected counts was examined.

Flood phantom SPECT study

A flood phantom SPECT study was performed to evaluate the uniformity of the reconstruction images. The phantom used in this study was the same one as the cylindrical phantom used to evaluate the linearity of count rate, and was filled with uniform ^{99m}Tc solution. The pinhole collimator with 1-mm diameter was used. The ROR was 30 mm. This resulted in a magnification factor of 1.32. Projection data of 120 views were acquired over 360° using step and shoot acquisition; 10 sec/step, 3° increments. Decay correction and the above-mentioned pinhole sensitivity correction were applied for projection data before reconstruction. The projection data were reconstructed using our previously validated pinhole 3D-OSEM method employing a 3D voxel-driven projector in both back- and forward-projections with eight subsets and two iterations. The corrections for attenuation, scatter and penetration were not done.

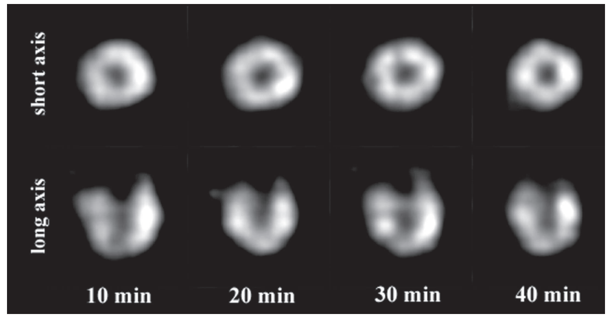

Fig. 8 Short- and long-axial images of rat myocardial perfusion obtained by sequential SPECT scans. The left ventricular walls and cavities were clearly visible in all of four frames obtained for 40 min.

Animal SPECT study

Rat myocardial perfusion SPECT scans were sequentially performed. A male rat weighing 220 g was anesthetized with sodium pentobarbital and held vertically on the object rotating stage, and then was scanned after intravenous 2-min administration of 6.21 MBq/1.5 ml ^{201}TlCl into the tail vein. The pinhole of 1 mm was used. The ROR was 30 mm. Scans for 10 min were sequentially performed four times using 360° step and shoot acquisition; 5 sec/step, 3° increments. Like the flood phantom study, projection data were reconstructed using our pinhole 3D-OSEM method with eight subsets and two iterations. Corrections for attenuation, scatter, penetration and pinhole sensitivity were not performed.

RESULTS

Basic system performances

(1) Energy resolution: Figure 6 (a) shows a sample energy spectrum from one crystal near the center of the detector block. The energy resolution was 20.8-keV (14.8%) FWHM at 140 keV.

(2) System spatial resolution: Figure 6 (b) shows a planar image profile of the ^{99m}Tc line source. The spatial resolutions were 2.8-mm FWHM and 2.5-mm FWHM for ^{99m}Tc and ^{201}Tl, respectively.

(3) Sensitivity: Figure 6 (c) shows system sensitivity on the central axis as a function of distance from the pinhole for ^{99m}Tc with 0.5- and 1.0-mm pinholes and for ^{201}Tl with 1.0-mm pinhole. The sensitivity of ^{201}Tl was slightly smaller than that of ^{99m}Tc. In the case of ^{99m}Tc, the sensitivities at a pinhole-source distance of 30 mm were 27.0 and 53.0 cps/MBq with 0.5-mm and 1.0-mm pinholes, respectively. In the case of ^{201}Tl, the sensitivity at the same distance was 49.1 cps/MBq with the 1.0-mm pinhole.

(4) Linearity of count rate: Figure 6 (d) shows the relationship between the source activity and the count rate. The linearity was good up to 10 kcps and the regression line was $y = 0.0588x + 0.009$ ($r^2 = 0.9999$). However, the ratio of the count rate to the source activity gradually decreased over 10 kcps.

Flood phantom SPECT study

Figure 7 shows SPECT images of uniform cylindrical phantom. The image reconstructed with pinhole geometrical sensitivity correction was almost uniform, while the image without the correction had high counts around the center and low counts at the periphery.

Animal SPECT study

Figure 8 shows sequential SPECT images of a rat myocardial perfusion in four frames obtained for 40 min. The left ventricular walls and cavities were clearly visible in all frames.

DISCUSSION

We have developed a compact SPECT system using a compact pixellated gamma camera for small animals and succeeded in sequential SPECT imaging of rat myocardial perfusion. In this system we employed 2″ PSPMT rather than 5″ PSPMT which was used by other investigators[21–23] because the use of 2″ PSPMT allows one to construct a more inexpensive, compact and lighter system.

The energy resolution of 14.8% FWHM in this camera was worse than that of approximately 10% FWHM in clinical SPECT gamma camera. So, the profile of the photopeak in the energy spectrum was as broad as the 36% energy window used. McElroy et al. reported[22] that in their pinhole system, scatter fraction did not contribute a significant amount to images (about 5%) for mouse sized 2.5-cm diameter cylinder when the usual 20% energy window was used in their system with a 11.4% energy resolution. However, the scatter fractions were about 15% and 20% for rat sized 3.8-cm and 5.05-cm diameter cylinders. Further study is needed to evaluate the contribution of scatter photons and develop proper scatter correction technique[26] for our system.

The measured system spatial resolutions were 2.8-mm FWHM and 2.5-mm FWHM for ^{99m}Tc and ^{201}Tl, respectively. Here, the theoretical system spatial resolution for a pinhole collimated gamma camera R_0 is given by

$$R_0 \cong \sqrt{\left(\frac{b}{f}R_i\right)^2 + \left(d_e\frac{f+b}{f}\right)^2}, \quad (3)$$

where f is the distance between the pinhole and the detector (focal length), b is ROR, R_i is the intrinsic camera resolution, and d_e is the effective pinhole diameter expressed as:

$$d_e \approx \sqrt{d\left[d + \frac{2}{\mu}\tan\left(\frac{\alpha}{2}\right)\right]}, \quad (4)$$

where d is the actual pinhole diameter, μ is the linear attenuation coefficient of the collimator material, and α is the opening angle of the pinhole collimator.[22,27] The theoretical spatial resolutions in this experimental condition are 2.5 mm and 2.3 mm for ^{99m}Tc and ^{201}Tl, respectively. The spatial resolution of ^{99m}Tc is larger than that of ^{201}Tl due to its higher energy ($\mu \approx 4.098$ mm^{-1} for ^{99m}Tc and $\mu \approx 20.870$ mm^{-1} for ^{201}Tl) and more penetration photons, which appeared in the experimental results. However, the measured spatial resolutions are slightly worse than the theoretical ones. As one of the reasons for the difference, the theoretical calculation assumes a double knife-edge pinhole collimator, while our pinhole collimator is single knife-edge. The number of penetration photons in single knife-edge is larger than that in double knife-edge. Therefore, the actual pinhole diameter for single knife-edge is larger than that for double knife-edge. By accounting for the difference of the knife-edge of the collimator, the measured spatial resolutions largely agree with the theoretical ones. Weber et al. obtained rat myocardial images at a spatial resolution of 2.8-mm FWHM.[11] The spatial resolution measured in our system is almost equal to that measured in their system.

However, the spatial resolution obtained in our system might be unsatisfactory for mouse imaging. Resolution can be improved by using a smaller diameter pinhole, but this will decrease sensitivity in return for improvement of resolution. Decreasing the crystal size or enlarging the detection area of the camera can improve resolution without decreasing sensitivity. Resolution is usually degraded by non-zero diameter and edge penetration of a pinhole. Alternatively, this degraded resolution can be recovered by incorporating the realistic pinhole model into reconstruction software.[28,29] This approach does not require any modification of hardware and is applicable to our system.

From Figure 6 (c), positioning the pinhole closer to the object is important for improvement of sensitivity in pinhole SPECT. In that respect, the flat face of a single-knife edge collimator is advantageous. However, care must be taken of the effect of penetration for thin, single knife-edge collimator. The sensitivity of ^{201}Tl was slightly smaller than that of ^{99m}Tc. This is considered that the number of penetrations for ^{201}Tl was less than that for ^{99m}Tc due to lower energy of ^{201}Tl compared to ^{99m}Tc. In future we need to evaluate the effect of the penetration for both ^{99m}Tc and ^{201}Tl in single-knife edge.

A good linearity of the count rate up to 10 kcps was shown in this study, although the ratio of the count rate to the source activity gradually decreased over 10 kcps. This characteristic of the count rate allows the present compact gamma camera system to be applied for rat myocardial

SPECT imaging with ^{201}Tl because the mean count rate was 0.52 kcps during SPECT data acquisition in this rat study. This upper limitation of 10 kcps is due to the transfer speed of the electric circuit which can be improved by replacement with faster electronics. The present system also produced homogeneous reconstructed images of the cylindrical phantom as shown in Figure 7. The homogeneity of images reconstructed from the flood phantom is important for quantitative analysis of physiological function.

In the animal SPECT study, rat myocardial tomographic images were sequentially obtained. The SPECT images could clearly visualize the rat myocardium and cardiac cavity. It is anticipated that these images could be significantly improved if image gate is employed. The time-dependent change of regional tissue radioactivity concentration obtained from such sequential tomographic images can be applied for kinetic analysis using a compartment model to estimate the regional myocardial blood flow.[30] The results for phantom and animal studies support the feasibility of our system for quantitative assessments of regional myocardial blood flow on rat. Further study is needed to quantify myocardial blood flow by pinhole SPECT. Deloar et al. suggested that physical factors such as penetration and scatter are considered.[31] Also, Wang et al. reported that both of attenuation correction (AC) and scatter compensation (SC) are important to improve quantitative accuracy because the values of reconstructed images were underestimated by 15% without AC and overestimated by 9% with only AC, while the quantitative accuracy was below 3% with both AC and SC.[32]

If this compact camera is combined with a rotating apparatus, the camera will rotate around the animal laid down. So, we can observe physiological function of small animals in more natural conditions, against especially acquiring complete data set with two orbits,[18] than when the animals are held vertically like in this study. The misalignment of a center of rotation (COR) might be a problem, if the camera is rotated. It causes serious artifacts in the reconstructed image.[13] However, our compact camera is sufficiently light to avoid the misalignment of the COR compared to clinical gamma camera. In the near future, we will construct a small animal pinhole SPECT system, which permits acquisition of complete data by two-circular orbit, using a compact gamma camera.

CONCLUSION

We have developed a compact SPECT system using a compact pixellated gamma camera for small animals. The camera with an active detection area of 43.8 mm × 43.8 mm was equipped with a pinhole collimator. We evaluated the basic physical performances and succeeded in sequential SPECT imaging of rat myocardial perfusion. The present system may be of use for quantitation of biological functions such as myocardial blood flow in small animals.

ACKNOWLEDGMENT

This study was financially supported by the Budget for Nuclear Research of the Ministry of Education, Culture, Sports, Science and Technology, based on screening and counseling by the Atomic Energy Commission, Japan.

REFERENCES

1. Meikle SR, Eberl S, Iida H. Instrumentation and methodology for quantitative pre-clinical imaging studies. *Curr Pharm Des* 2001; 7 (18): 1945–1966.
2. Chatziioannou AF. PET scanners dedicated to molecular imaging of small animal models. *Mol Imaging Biol* 2002; 4 (1): 47–63.
3. Hirai T, Nohara R, Ogoh S, Chen LG, Kataoka K, Li XH, et al. Serial evaluation of fatty acid metabolism in rats with myocardial infarction by pinhole SPECT. *J Nucl Cardiol* 2001; 8 (4): 472–481.
4. Scherfler C, Donnemiller E, Schocke M, Dierkes K, Decristoforo C, Oberladstätter M, et al. Evaluation of striatal dopamine transporter function in rats by *in vivo* β-[^{123}I]CIT pinhole SPECT. *NeuroImage* 2002; 17: 128–141.
5. Acton PD, Choi SR, Plössl K, Kung HF. Quantification of dopamine transporters in the mouse brain using ultra-high resolution single-photon emission tomography. *Eur J Nucl Med* 2002; 29 (5): 691–698.
6. Aoi T, Watabe H, Deloar HM, Ogawa M, Teramoto N, Kudomi N, et al. Absolute quantitation of regional myocardial blood flow of rats using dynamic pinhole SPECT. In Conference Record of 2002 IEEE Nuclear Science Symposium and Medical Imaging Conference (CD-ROM), 2003: M11-185.
7. Jeavons AP, Chandler RA, Dettmar CAR. A 3D HIDAC-PET camera with sub-millimetre resolution for imaging small animals. *IEEE Trans Nucl Sci* 1999; 46 (3): 468–473.
8. Seidel J, Vaquero JJ, Green MV. Resolution uniformity and sensitivity of the NIH ATLAS small animal PET scanner: comparison to simulated LSO scanners without depth-of-interaction capability. *IEEE Trans Nucl Sci* 2003; 50 (5): 1347–1350.
9. Tai YC, Chatziioannou AF, Yang Y, Silverman RW, Meadors K, Siegel S, et al. MicroPET II: design, development and initial performance of an improved microPET scanner for small-animal imaging. *Phys Med Biol* 2003; 48: 1519–1537.
10. Jaszczak RJ, Li J, Wang H, Zalutsky MR, Coleman RE. Pinhole collimation for ultra-high-resolution, small-field-of-view SPECT. *Phys Med Biol* 1994; 39: 425–437.
11. Weber DA, Ivanovic M, Franceschi D, Strand SE, Erlandsson K, Franceschi M, et al. Pinhole SPECT: an approach to *in vivo* high resolution SPECT imaging in small laboratory animals. *J Nucl Med* 1994; 35 (2): 342–348.
12. Ishizu K, Mukai T, Yonekura Y, Pagani M, Fujita T, Magata Y, et al. Ultra-high resolution SPECT system using four pinhole collimators for small animal studies. *J Nucl Med* 1995; 36 (12): 2282–2287.

13. Ogawa K, Kawade T, Nakamura K, Kubo A, Ichihara T. Ultra high resolution pinhole SPECT for small animal study. *IEEE Trans Nucl Sci* 1998; 45 (6): 3122–3126.
14. Moore SC, Zimmerman RE, Mahmood A, Mellen R, Lim CB. A triple-detector, multiple-pinhole system for SPECT imaging rodents. [Abstract] *J Nucl Med* 2004; 45 (suppl): 97–98.
15. Beekman FJ, van der Have F, Vastenhouw B, van der Linden AJ, van Rijk PP, Burbach JP, et al. U-SPECT-I: a novel system for submillimeter-resolution tomography with radiolabeled molecules in mice. *J Nucl Med* 2005; 46 (7): 1194–1200.
16. Sun M, Izaguirre EW, Funk T, Hwang AB, Carver J, Thompson S, et al. A CdZnTe-based high-resolution microSPECT system. [Abstract] *J Nucl Med* 2005; 46 (suppl 2): p170.
17. Lackas C, Hoppin JW, Schramm NU. Performance analysis of a submillimeter-resolution multi-pinhole SPECT small-animal imaging system. [Abstract] *J Nucl Med* 2005; 46 (suppl 2): p171.
18. Zeniya T, Watabe H, Aoi T, Kim KM, Teramoto N, Hayashi T, et al. A new reconstruction strategy for image improvement in pinhole SPECT. *Eur J Nucl Med Mol Imaging* 2004; 31 (8): 1166–1172.
19. Liu Z, Kastis GA, Stevenson GD, Barrett HH, Furenlid LR, Kupinski MA, et al. Quantitative analysis of acute myocardial infarct in rat hearts with ischemia-reperfusion using a high-resolution stationary SPECT system. *J Nucl Med* 2002; 43 (7): 933–939.
20. Schramm NU, Ebel G, Engeland U, Schurrat T, Béhé M, Behr TM. High-resolution SPECT using multipinhole collimation. *IEEE Trans Nucl Sci* 2003; 50 (3): 315–320.
21. Schramm N, Wirrwar A, Sonnenberg F, Halling H. Compact high resolution detector for small animal SPECT. *IEEE Trans Nucl Sci* 2000; 47 (3): 1163–1167.
22. McElroy DP, MacDonald LR, Beekman FJ, Wang Y, Patt BE, Iwanczyk JS, et al. Performance evaluation of A-SPECT: a high resolution desktop pinhole SPECT system for imaging small animals. *IEEE Trans Nucl Sci* 2002; 49 (5): 2139–2147.
23. Wojcik R, Goode AR, Smith MF, Beller GA, Ellman PI, Majewski S, et al. Dedicated small field of view SPECT system based on a 5″ PSPMT and crystal scintillator array for high resolution small animal cardiac imaging. In Conference Record of 2003 IEEE Nuclear Science Symposium and Medical Imaging Conference (CD-ROM), 2004: M3-43.
24. Smith MF, Jaszczak RJ. The effect of gamma ray penetration on angle-dependent sensitivity for pinhole collimation in nuclear medicine. *Med Phys* 1997; 24 (11): 1701–1709.
25. Metzler SD, Bowsher JE, Smith MF, Jaszczak RJ. Analytical determination of pinhole collimator sensitivity with penetration. *IEEE Trans Med Imag* 2001; 20 (8): 730–741.
26. Deloar HM, Watabe H, Kim KM, Aoi T, Kunieda E, Fujii H, et al. Optimization of the width of the photopeak energy window in the TDCS technique for scatter correction in quantitative SPECT. *IEEE Trans Nucl Sci* 2004; 51 (3): 625–630.
27. Anger HO. Radioisotope cameras. In: *Instrumentation in nuclear medicine*, Hine GJ (ed), New York; Academic, 1967: 485–552.
28. Bequé D, Vanhove C, Andreyev A, Nuyts J, Defrise M. Correction for impact camera motion and resolution recovery in pinhole SPECT. In Conference Record of 2004 IEEE Nuclear Science Symposium and Medical Imaging Conference (CD-ROM), 2005: M2-173.
29. Cao Z, Bal G, Acton PD. Pinhole SPECT reconstruction with resolution recovery. [Abstract] *J Nucl Med* 2005; 45 (suppl 2): 109–110.
30. Iida H, Eberl S. Quantitative assessment of regional myocardial blood flow with thallium-201 and SPECT. *J Nucl Cardiol* 1998; 5: 313–331.